Lab on a Chip

Accepted Manuscript

This article can be cited before page numbers have been issued, to do this please use: M. Rafeie, J. Zhang, M. Asadnia, W. Li and M. Ebrahimi Warkiani, *Lab Chip*, 2016, DOI: 10.1039/C6LC00713A.

ROYAL SOCIETY OF CHEMISTRY

www.rsc.org/loc

View Article Online
DOI: 10.1039/C6LC00713A

Multiplexing slanted spiral microchannels for ultra-fast blood plasma separation

Mehdi Rafeie[1#], Jun Zhang[2#], Mohsen Asadnia[3], Weihua Li[2] and Majid Ebrahimi Warkiani[1]*

[1]School of Mechanical and Manufacturing Engineering, Australian Centre for NanoMedicine, University of New South Wales, Sydney, NSW 2052, Australia

[2]School of Mechanical, Materials and Mechatronic Engineering, University of Wollongong, Wollongong, NSW 2522, Australia

[3]Department of Engineering, Faculty of Science, Macquarie University, Sydney, NSW 2109, Australia

[#] These authors contributed equally to this work.

* Contact:

Majid Ebrahimi Warkiani (m.warkiani@unsw.edu.au)
School of Mechanical and Manufacturing Engineering, Australian Centre for NanoMedicine, University of New South Wales, Sydney, NSW 2052, Australia.

View Article Online
DOI: 10.1039/C6LC00713A

Abstract

Blood and blood products are critical components of health care. Blood components perform distinct functions in human body and thus the ability to efficiently fractionate blood into its individual components (i.e., plasma and cellular components) is of utmost importance for therapeutic and diagnostic purposes. Although conventional approaches like centrifugation and membrane filtration for blood processing have been successful in generating relatively pure fractions, they are largely limited by factors such as required blood sample volume, component purity, clogging, processing time and operation efficiency. In this work, we developed a high-throughput inertial microfluidic system for cell focusing and blood plasma separation from small to large volume blood samples (1-100 mL). Initially, polystyrene beads and blood cells were used to investigate the inertial focusing performance of a single slanted spiral microchannel as a function of particle size, flow rate, and the blood cells concentration. Afterwards, the blood plasma separation was conducted using the optimised spiral microchannel with relatively large dimensions. It was found that the reject ratio of the slanted spiral channel is close to 100% for blood samples with the haematocrit (HCT) of 0.5% and 1% under an optimal flow rate of 1.5 mL/min. Finally, through a unique multiplexing approach, we built a high-throughput system consisted of 16 spiral channels connected together which can process the diluted samples with a total flow rate as high as 24 mL/min. The proposed multiplexed system can surmount shortcomings of previously-reported microfluidic systems for plasma separation and cell sorting in terms of throughput, yield and operation efficiency.

View Article Online
DOI: 10.1039/C6LC00713A

1. Introduction

Blood is inarguably one of the most important biofluids used in medical laboratory diagnostics. Analysis of blood components are often used in healthcare to determine physiological and biochemical states, such as disease (e.g., cancer and infection), mineral content, and organ function.[1] Plasma and the blood cells are the two main constituents of the whole blood. Blood cells occupy approximately 40-45% volume of the blood in adults and comprise mainly of red blood cells (RBCs), which makes up more than 99% of the total blood cells.[1, 2] Blood plasma, which takes up the remaining 55% of the total volume of the whole blood, comprises of 95% water and various analytes, such as circulating nucleic acids, micro-organisms, proteins, and metabolites.[3] These analytes are of great importance in medical diagnostics. Hence, the separation of plasma from the blood plays an important role in diagnosis and monitoring various diseases.[1] For the effective detection of these analytes, the blood cells need to be removed completely so that they do not interface with the detection systems.[3, 4]

Although standard techniques for blood processing such as centrifugation and membrane filtration, which leverage on physical properties such as cell density and size, can provide effective separation of blood plasma, they are still largely limited by factors such as component purity, clogging, processing time and operation efficiency.[5] For example, centrifugation is generally labour-intensive, time-consuming, bulky, and even dangerous to some extent due to ultra-high speed rotating parts in working. The operator needs to be well-trained, with specialized knowledge and skill. Normally, plasma is manually pipetted from the centrifuge tube, and transferred for the downstream process. This inevitably entails human error, which may significantly alter subsequent results and cause inconsistent outcomes. The membrane filtration also suffers from the problem of severe clogging due to the finite filtration capacity, and frequent rinse is lab-intensive and unfavourable.[6] Moreover, the integration of these techniques into lab-on-a-chip (LOC) systems is very challenging.[7]

To address this unmet need, microfluidic based techniques have been gaining great attention in recent years as efficient and powerful approaches for high throughput blood cell separation, owing to their precise control of fluid behaviour at micro-scale.[5, 8] Microfluidic systems normally leverage on the disparities in the intrinsic properties of the different cell populations (i.e., size, deformability, surface charge, and density) to achieve separations and can be broadly classified as active and passive separation techniques.[9] Active techniques rely on an

View Article Online
DOI: 10.1039/C6LC00713A

external force field such as acoustic[10, 11] or magnetic[12, 13] for operation, while passive techniques depend only on the channel geometry and inherent hydrodynamic forces for functionality.[14] Generally, passive separation techniques are favored in comparison to active methods because they tend to avoid complicated integration of external force fields and they are cost effective.[15] Applications of both the active and passive microfluidic systems on the blood plasma separation have been recently reviewed by Kersaudy-Kerhoas and Sollier.[16] However, the volumetric flow rate of the most reported studies on the blood plasma extraction is still limited within the scale of μL/min,[4, 17-26] which is incompatible with the typical biosample volumes used in clinical setting.[27]

The abundant analytes in the plasma, such as cardiac markers and glucose dosage, are concentrated enough in a drop of the blood (~ 10 μL) to be exploited for an effective detection,[16] while in most situations, analytes, such as circulating DNA, are rare and their concentration is below a meaningful quantity for effective evaluation. Analytes then need to be concentrated, and a large volume (~ mL scale) of the blood sample needs to be processed within a reasonable time.[16] In addition, in a blood donation centre, plasma will be processed to produce a variety of products, which can be used to treat a number of potentially life-threatening conditions including burns, haemophilia, trauma and kidney diseases.[28] Consequently, a large volume of the blood sample needs to be processed to meet these needs.

Inertial microfluidics, which takes advantage of size-dependent hydrodynamic forces in microfluidic channels, has gained considerable interest in recent years for high-throughput cell sorting.[29] Mach and Di Carlo[26] presented a massively parallelized microfluidic device with 40 single straight microchannels placed in a radial array that passively separates pathogenic bacteria from diluted (1/100) blood. A removal efficiency of >80% pathogenic bacteria from blood was demonstrated with a high throughput of 400 million cells/min at the flow rate of 4 mL/min. Besides the removal of pathogenic bacteria from diluted blood, the device was also expected to be suitable for the blood plasma separation, stored blood filtration, and municipal water filtration. Our group have also developed a high-throughput device with 8 parallel serpentine channels to achieve a total flow rate of 2.8 mL/min and the throughput of almost 700 million cells/min, with the separation purity of ~99.75%.[30] However, these works on parallelization were mainly focused on a microchannel with linear structure, such as straight[26] and serpentine[30] channels. Spiral channels with complex nonlinear structure have been shown to be very promising for particle focusing and

View Article Online
DOI: 10.1039/C6LC00713A

separation,[31, 32] cell-in-droplet encapsulation,[33] cell-cycle synchronization,[34] blood cell sorting and plasma extraction,[35] circulating tumor cells (CTCs) isolation.[36, 37] Nivedita and Papautsky[35] reported a spiral devices to achieve blood cell separation as well as blood plasma extraction. In their work, 100× diluted blood (0.45% HCT) was processed at a flow rate of ~1 mL/min, and the collected blood plasma could reach ~100% cell-free. However, the separation efficiency was reduced to ~90% ± 3% when dilution factor decreased to 50× (0.9% HCT). Recently, Xiang and Ni[38] developed a spiral microfluidic device which can efficiently isolate blood plasma from 20× diluted whole blood at a flow rate of 700 µL/min. The purity of the isolated blood plasma was close to 100% and the yield was around 38.5%. However, in both works, the separation of blood plasma was conducted using a single spiral channel, it is yet difficult to implement a parallelization design to scale up the flow rate and throughput, especially along the planar direction.[6, 30, 39]

Our team has recently demonstrated the possibility of stacking spiral channels with rectangular cross-section for high throughput size-based separation and the retrieval of CTCs from peripheral blood.[39] Later on, we further improved the separation resolution of spiral devices while maintaining the high-throughput feature by modifying the shape of channel cross-section to be trapezoidal instead of conventional rectangular.[39, 40] In a spiral channel with trapezoidal cross-section, a sharp shift of particle focusing position from outer wall to inner wall was observed when exceeding a certain threshold of flow rate.[41] Given the fact that channel dimensions in conjunction with the applied flow rate dictate the focusing ability of the minimum particle size, this potentially limits the utility of these systems to the relatively large (> 6 µm) microparticles and biological cells. Here we extend our work to study the behaviour of small particles (~ 3-4 µm, mimicking the size of platelets[5]) in a slanted spiral channel, characterising focusing behaviour and separation efficiency at a range of flow rates up to 3000 µL/min (for a single spiral). Additionally, we developed a unique strategy to connect many spirals together along the planar and vertical directions, and demonstrated its application for ultra-fast blood plasma separation (24 mL/min). To maintain an equal input flow condition for each parallel spiral channel, a novel plastic guide layer was designed and fabricated by 3D printing technology to connect and seal the inlets of the spiral channels. The proposed strategy is also applicable to multiplexing the design along the height direction to further boost the total throughput. The utility of this system was showcased for high-throughput plasma separation from small to large volume blood samples (1-100 mL). We

View Article Online
DOI: 10.1039/C6LC00713A

believe that this method of cell separation (and fractionation) can be adopted easily in clinics and hospitals for high throughput blood sample processing.

2. Theory

2.1 Inertial migration

Inertial migration is a phenomenon where randomly dispersed particles in the entrance of a channel migrate laterally to several equilibrium positions within the cross-section of the channel.[42, 43] The inertial migration phenomenon has been widely recognised by the counteraction of two inertial effects: i) shear gradient lift force F_{LS}; due to the parabolic curvature of the fluid velocity profile and its interaction with particles, which directs the particles away from channel centre, and ii) wall lift force F_{LW}; considered as a result of the flow field interaction between the suspending particles and the adjacent walls, which repels the particles away from the wall.

In a straight microchannel, the inertial focusing of particles is done through two steps. In the first step, the particles/cells are affected by F_{LS} and F_{LW}, and propelled towards equilibrium lines where these two inertial lift forces are in balance as shown in Fig. 1A-D. In a circular channel, the equilibrium positions are normally located around 0.6 times channel radius from the channel centreline (Fig. 1A).[43, 44] In a square channel, the equilibrium lines are located parallel to the channel walls (Fig. 1B).[45] By increasing or decreasing the aspect ratio of the cross-section of a rectangular channel, the gradient of the parabolic velocity will become stronger along the shorter side and cause the equilibrium positions to locate along larger sides only (Fig. 1C).[45] In a trapezoidal channel, it is believed that the equilibrium lines remain parallel to the channel walls; however, similar to the case of a high/low aspect ratio rectangular channel, an equilibrium line parallel to the channel wall may not be formed near the shorter side of the channel. During the second step of the inertial focusing, while particles have already focused on the equilibrium lines, they are also known to slowly assemble around the centre of the channel walls under the influence of the Saffman lift force $F_{L\Omega}$ [46, 47] originated from the rotation of the particles/cells (Fig. 1E-H).

The net inertial lift force F_L can be expressed as follows where the particle size is small compared to the channel size:[48, 49]

View Article Online
DOI: 10.1039/C6LC00713A

$$F_L = \frac{\rho U^2 a^4}{{D_h}^2} f_L(Re, z_C) \quad (1)$$

$$Re = \frac{\rho U D_h}{\mu} \quad (2)$$

in which ρ, U and μ are fluid density, maximum velocity, and dynamic viscosity respectively; a is the particle diameter, and D_h is the hydraulic diameter of the channel. $f_L(Re, z_C)$ is the lift coefficient of the net inertial lift force, which is a function of normalized position of the particles within cross-section of the channel z_C, and the Reynolds number Re.[49]

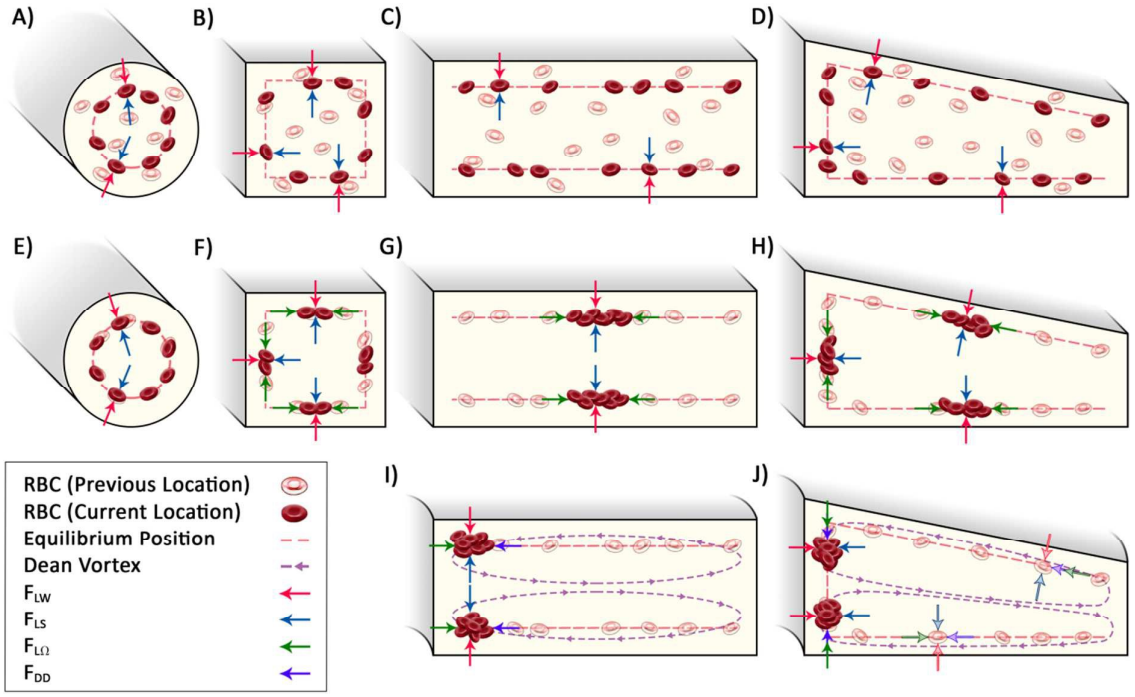

Fig. 1 Schematic illustration of cell focusing in straight and curved microchannels. (**A-D**) In a straight channel with circular, square, low aspect ratio rectangular, or trapezoidal cross-section, randomly dispersed particles/cells focus on equilibrium lines where F_{LS} and F_{LW} are in balance. (**E-H**) In a straight channel and assuming a relevant flowrate and concentration, particles/cells focus in the middle of the channel walls on previously formed equilibrium lines due to the Saffman lift force $F_{L\Omega}$. (**I**, **J**) In a curved channel, a centrifugal force acts on the fluid towards the outer wall and induces the creation of Dean vortices along the cross-section. These vortices relocate the equilibrium positions commonly towards the inner wall of the channel where particle/cells can remain on the equilibrium lines.

2.2 Secondary flow

By adding a curvature to the channel, the magnitude of the velocity of the fluid flowing near the outer wall will be more than that of near the inner wall because a longer distance needs to

View Article Online
DOI: 10.1039/C6LC00713A

be passed by the fluid near the outer wall (Fig. 2). The difference between the speed of the fluid near the inner and outer wall is succeeded by a pressure gradient along the radial direction which gives rise to a secondary flow driving the fluid from the inner wall to the outer wall of the channel, and entails a circulation to meet the continuity of the fluid. As a result, two counter rotating vortices form which are known as Dean vortices (Fig. 1I, J).[49] The magnitude of the secondary flow U_D can be approximated as:[31, 33]

$$U_D = 1.8 \times 10^{-4}\, De^{1.63} \tag{3}$$

where Dean number De is a function of the Reynolds number Re, the hydraulic diameter of the channel D_h, and the radius of the channel curvature R:[50]

$$De = \sqrt{\frac{D_h}{2R}}\, Re \tag{4}$$

Assuming the Stokes' drag law, the Dean drag force F_D can be evaluated as[51]

$$F_D = 3\pi\mu a U_D \tag{5}$$

Hence, the introduction of the channel curvature induces the secondary flow drag as an additional lateral force which can modify and assist the inertial focusing progress.[52] The focusing pattern (i.e., the position, number, and band width of the particle equilibrium positions) can be analysed by contemplating the balance between the secondary flow drag and the inertial lift force.[49] Depending on the flow rate, the Dean drag force may either be stronger or weaker than the Saffman or inertial lift force. As can be seen in Fig. 1J, while the Dean drag force is weaker than inertial lift forces but stronger than the rotation induced lift force, suspended particles/cells follow the Dean vortices along the equilibrium lines until they reach an area close to the inner wall where they cannot follow the vortices anymore.[53] Consequently, they accumulate near the inner wall and reduce the equilibrium positions to this region only, which is ideal for the separation purpose.

View Article Online
DOI: 10.1039/C6LC00713A

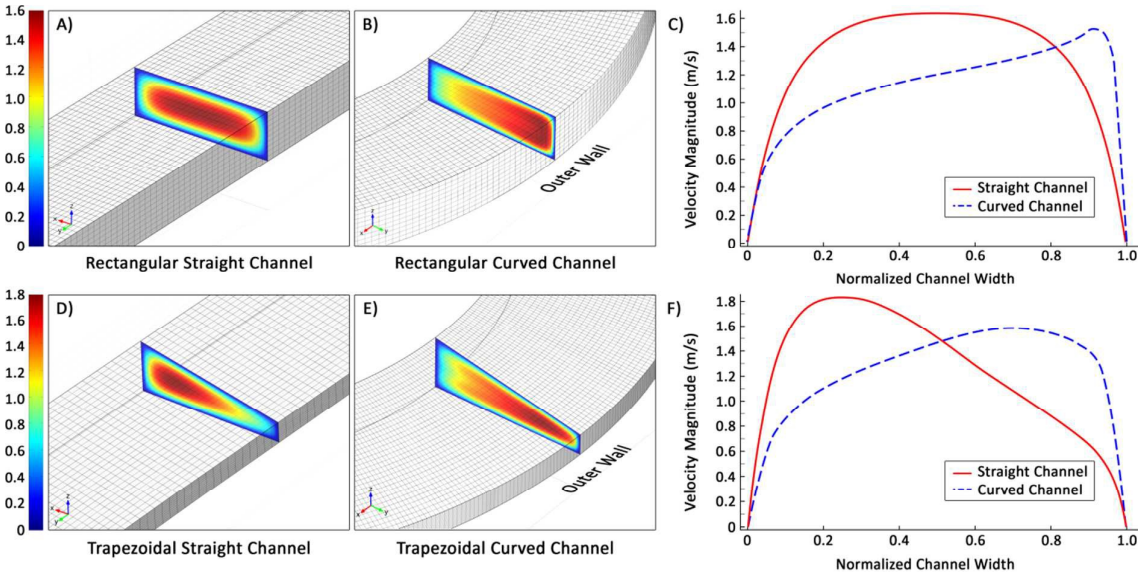

Fig. 2 Simulation results obtained using COMSOL Multiphysics® software. (**A**-**C**) The comparison of velocity contours in rectangular straight and curved channels reveals that the velocity near the outer wall of the curved channel increases to let the fluid pass a longer distance. Therefore, the maximum of the symmetric parabolic velocity profile in the straight channel deviates towards the outer wall in the curved channel. (**D**-**F**) In contrast to the rectangular channel, the maximum of the velocity profile in the trapezoidal straight channel locates near the longer side-wall. In the trapezoidal curved channel, however, the fluid velocity near the outer wall surpasses that of near the inner wall, regardless of whether the inner side-wall is shorter or longer. Such an alteration in the velocity profile in trapezoidal channels allows formation of stronger Dean flow in comparison to rectangular channels, which bestows higher inertial separation potential to trapezoidal channels.

2.3 Inertial focusing in a spiral channel with trapezoidal cross section

In a spiral microchannel with a trapezoidal cross-section, the asymmetry of the trapezoid influences the velocity profile and results in the formation of strong Dean vortex cores near the wall that has a larger channel depth.[41] Within a certain flow rate range, the modified velocity field of the trapezoidal spiral channel traps particles within the strong Dean vortex cores.[39] In this work, the height of the inner wall is much larger than that of the outer wall in comparison to our previous works.[39] The reason for designing such a cross-section was to dedicate more space to cells to accumulate near the inner wall. In addition, in a spiral channel with the same back pressure at the outlets, the volumetric flow rate near the outer wall would be naturally higher than that of the inner wall[54]. Thus, we designed the outlet channels, bifurcation position, and the cross-section of the chip in a way to accommodate higher number of cells (near inner wall with bigger size) while collecting larger volume of plasma from outer wall. Given the limitation of micromilling approach for manufacturing of the

View Article Online
DOI: 10.1039/C6LC00713A

master mold, we managed to build microchannels with bifurcation point closer to the inner wall that give us around 50% yield in plasma separation in one cycle (Table S5).

The parameter a/D_h referred as confinement ratio (CR) play a key role in focusing behaviour of particles both in straight and curved microchannels. It has been shown that particle focusing is normally happen at $CR \geq 0.07$.[46,55-59] Recently, the migration dynamics of particles with various confinement ratios was characterized in three different modes, namely focusing mode ($CR \geq 0.07$), rough focusing mode ($0.01 < CR < 0.07$), and non-focusing mode ($CR < 0.01$).[60] Here, the hydraulic diameter of the trapezoidal channel is $D_h = 4A/P = 99.02$ µm requiring the particle/cell diameter to be at least $a_{min} = 6.93$ µm. However, we could successfully focus (see section 4) and separate smaller particles and platelets (~ 3-4 µm) which refute the criterion of $CR \geq 0.07$ unless we consider some other characteristic length for a trapezoidal microchannel. Channel depth is commonly presumed to be the characteristic length of non-circular microchannels.[47, 61] Thus, taking the average of channel depth as the characteristic length results in $a_{min} = 3.85$ µm, which is in good agreement with our experiments.

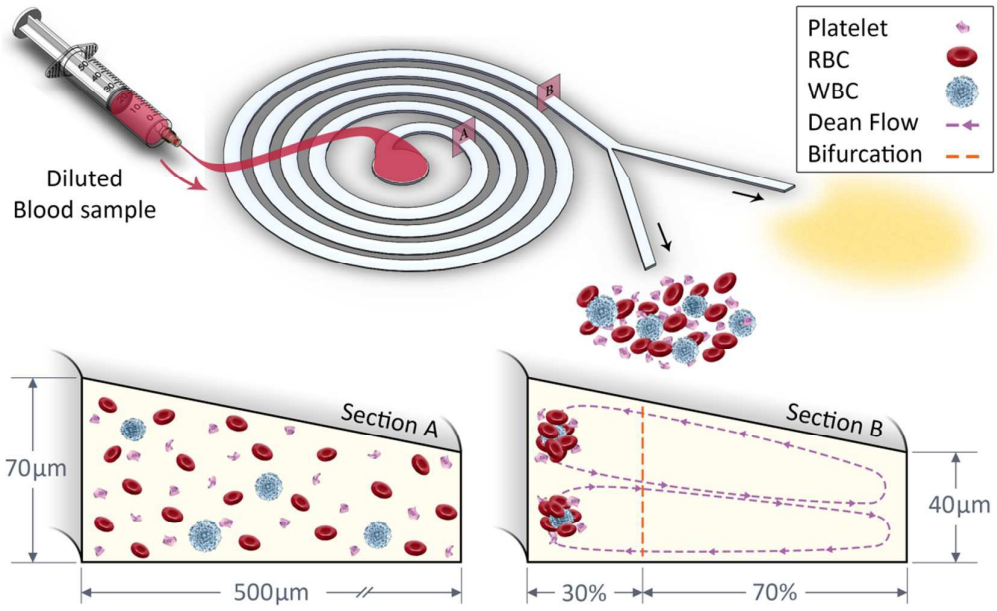

Fig. 3 Schematic illustration of the blood plasma separation using a spiral channel with a trapezoidal cross-section. Under the influence of inertial lift and Dean drag forces, blood cells are focused and concentrated near the inner wall around the vortex cores, and blood plasma is collected from the cell free region (outer wall). The bifurcation point is positioned closer to the inner wall to facilitate large volume of plasma collection.

View Article Online
DOI: 10.1039/C6LC00713A

3. Materials and methods

3.1 Design and fabrication

To determine the optimal flow rate for the plasma separation, a microfluidic device with a single spiral channel was first fabricated to examine particle focusing quality and position. Afterwards, a parallelized microfluidic device with eight spiral channels was fabricated and tested. All the trapezoidal cross-sectional spiral channels were made of polydimethylsiloxane polymer (PDMS, Sylgard 184 Silicone Elastomer Kit, Dow Corning) using soft lithography technique from an aluminium mould. The aluminium mould was manufactured using the micro-milling technique (Whits Technologies, Singapore) which precisely milled a positive print of the spiral microchannels. The degassed PDMS, mixed in a 10:1 ratio of the base and the curing agent, was poured onto the aluminium mould and peeled off after baking for 2 hours inside an oven at 70°*C*. The fluidic access holes were punched using a Uni-Core™ Puncher (Sigma-Aldrich Co. LLC. SG). The final device was irreversibly bonded with a thick PDMS slab using oxygen plasma cleaner (PDC-002, Harrick Plasma, Ossining, NY). Each spiral channel has four circular loops, one inlet, and two outlets. The slanted spiral channels have a trapezoidal cross-section with a width of 500 μm, and the inner and outer height of 70 μm and 40 μm respectively. For the parallelized microfluidic device, a 3D printing machine (SLA stereolithography system, USA) was utilised to fabricate a plastic guide layer which could connect and seal efficiently the input ports of the spiral channels delivering equal flows into each spiral microchannel.

3.2 Sample preparation

To build the multiplex system based on the single spiral microchannels, we characterized the performance of a single channel using fluorescent microbeads of 3.0, 4.16, and 9.9 μm as a surrogate for platelets, red blood cells and white blood cells in order to determine the optimal flow condition for cell filtration. Fluorescently labelled microbeads (Fluoresbrite® Microspheres, Polysciences Inc, Singapore) were added (0.01% volume fraction) to a sample buffer which consists of 1× phosphate buffered saline (PBS), and 2 mM EDTA supplemented with 0.5% bovine serum albumin (BSA) (MiltenyiBiotec, Germany). BSA was used to prevent the non-specific adhesion of microbeads to the tubing and microchannel walls.

View Article Online
DOI: 10.1039/C6LC00713A

3.3 Blood sample

Human whole blood samples were obtained from 5 healthy donors for our tests. This study was approved by our institutional review board and local ethics committee according to a protocol permitted by the Institutional Review Board (IRB). The human whole blood was taken from healthy adult volunteers with a vacutainer tube (i.e., Vacuette) containing anticoagulant agent K2EDTA to prevent the aggregation of blood cells. The blood sample was diluted 9, 22.5, 45 and 90 times using PBS before infused into the spiral microfluidic channels.

3.4 Experimental setup

The single spiral microfluidic device was mounted on an inverted phase contrast/epifluorescence microscope (Olympus IX81, Olympus Inc., USA) equipped with a 12-bit EMCCD camera (iXonEM + 885, Andor Technology, USA). Samples were loaded into a syringe and pumped through the microchannel at varying flow rates using a syringe pump (Harvard Apparatus PHD 2000, Harvard Apparatus Inc., USA). Images were acquired using Metamorph® software (Molecular Devices, USA) and analysed using ImageJ® software. The flow rate was ranging from 0.5 to 3 mL/min, and the effectiveness of the particle focusing was observed to ascertain the optimal flow rate for the blood cells filtration and the plasma extraction. Furthermore, blood cells concentrations in the collected plasma were measured by a haemocytometer to evaluate the separation performance.

4. Results and discussions

4.1 Characterization of inertial focusing in the slanted spiral channels by fluorescent microbeads

Before the implementation of the parallelization design, a microfluidic device with a single slanted spiral channel was designed, fabricated and tested using suspensions of differently-sized fluorescent particles at different flow rates. The purpose was to characterise the performance of particle inertial focusing at the bifurcation of the spiral channel at each flow rate. Through this way, an optimal flow rate for the separation of blood plasma can be estimated by the evaluation of the focusing behaviour of the polystyrene microbeads in terms of their distribution and position along the channel width.

View Article Online
DOI: 10.1039/C6LC00713A

The particle focusing phenomenon can be easily observed through the consecutive loops of the spiral channel within the microfluidic device. As depicted in Fig. 4A, initially, particles are randomly distributed at the inlet, and migrate laterally towards the inner wall of the spiral channel as they progress through the loops. Finally, they focus as a narrow band near the inner wall. As can be seen in Fig. 4C, 3.0 µm particles, which are slightly smaller than a_{min} = 3.85 µm, roughly focus near the inner wall meaning that a portion of these particles at all the flow rates remain dispersed along the channel width. In addition, a higher portion of the microbeads become unfocused by increasing the flow rate. The 9.9 µm particles, however, have a distinguishable single focusing trace at flow rates ranging from 0.5 to 2 mL/min, while they become dissipated at flow rates higher than 3 mL/min which let a portion of the particles exit from the outer wall of the channel. We infer that at these flow rates, the Dean drag force dominates the inertial lift forces giving rise to the particles to leave the equilibrium lines near the inner wall and continue following the strong counter-rotating Dean vortices.

The focusing behaviour trend of 4.16 µm particles is quite similar to their large counterparts, namely 9.9 µm particles. However, at the flow rate of 0.5 mL/min, the Dean drag force and the net inertial lift force exerting on 4.16 µm particles have almost the same magnitude, leading some particles to get trapped by the inertial lift forces while the rest of them still follow the secondary flow. As can be seen in Fig. 4C, at the same flow rate, the difference between the Dean drag force and inertial lift force experienced by larger particles is less than that of the smaller microbeads. This situation also happens at 3 mL/min where 4.16 µm particles are more dispersed compared to 9.9 µm particles implying that the effective range of the flow rates at which smaller particles can focus in a microchannel is relatively narrower than that of the larger particles. It proves that the net inertial lift force increases much more than the Dean drag force with the increase of the particle size, which is consistent with the force analysis obtained from the equations (1) and (5) stating that $F_L \sim a^4$ and $F_D \sim a$. Having analysed the results of the polystyrene beads tests, we concluded that the flow rates between 1.5 and 2 mL/min are optimal for effective particle focusing in the designed slanted spiral channels, and this range would be suitable for the blood plasma separation.

View Article Online
DOI: 10.1039/C6LC00713A

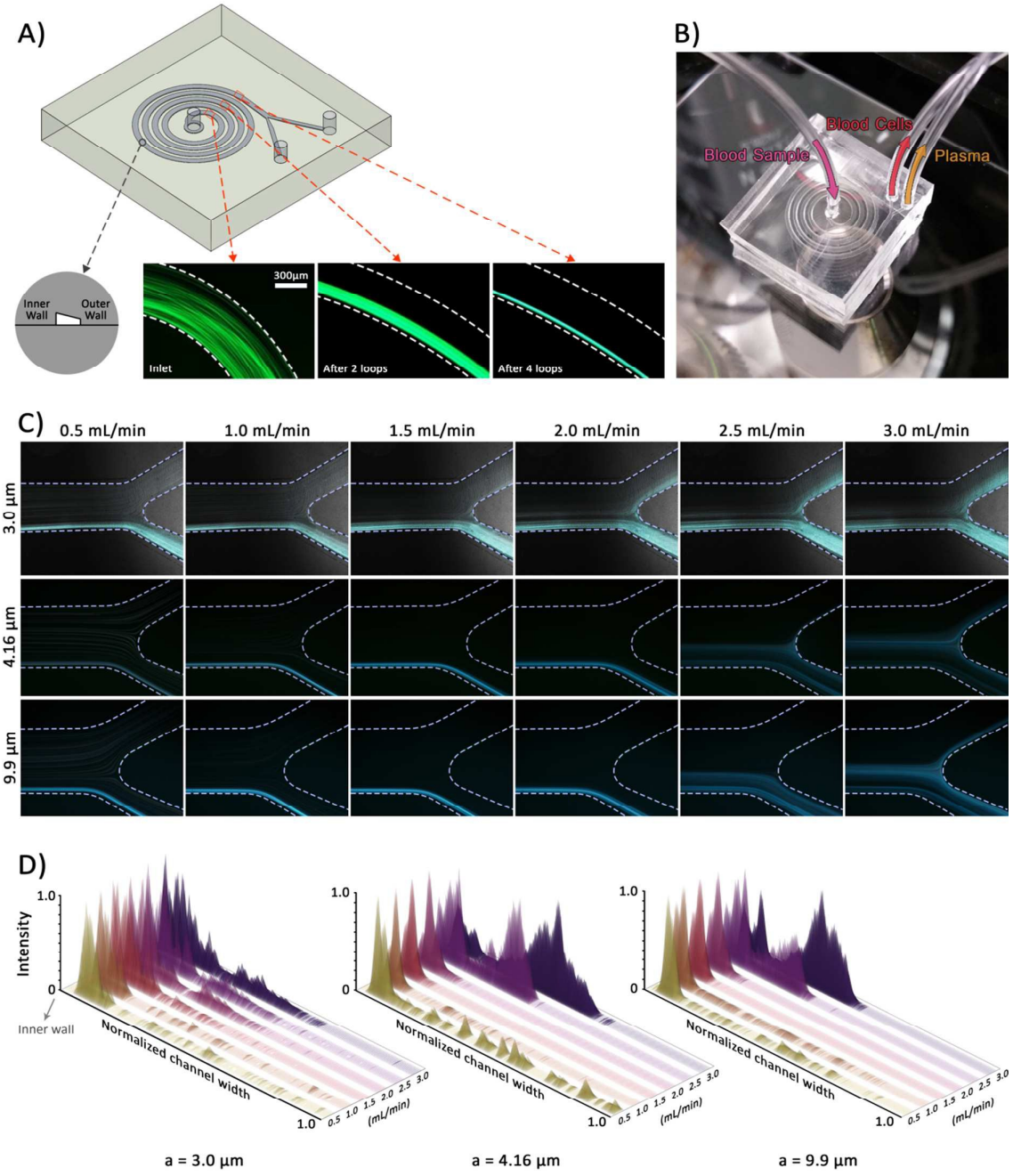

Fig. 4 (**A**) A composite image showing inertial focusing of fluorescent particles in different loops of the slanted spiral channel. (**B**) Optical picture of a single spiral microchannel placed on the microscope. (**C**) The inertial focusing of 3.0, 4.16 and 9.9 μm fluorescent beads at the outlet of the slanted spiral channel under flow rates ranging from 0.5 to 3 mL/min. (**D**) The normalized intensity profile of the fluorescent particles along the width of the channel. The 3.0 μm particles roughly focus while 4.16 and 9.9 μm can focus completely near the inner channel wall. Additionally, all the particles tend to shift towards the outer wall when flow rates increases. The flow rates between 1.5 and 2.0 mL/min provide the best inertial focusing among the working flow rate range.

View Article Online
DOI: 10.1039/C6LC00713A

4.2 Characterization of the separation performance with blood samples

Since the optimal flow rate of the inertial focusing for both the 4.16 and 9.9 μm particles varies from 1.5 to 2 mL/min, and 3.0 μm particles are mainly focused near the inner wall at these flow rates, 1.5 mL/min was selected for the blood plasma separation. Human whole blood was drawn from a healthy male donator and diluted from 9 to 90 times by PBS. We investigated the migration behaviour of blood cells along the different loops of the slanted spiral channel as shown in Fig. 5A. The focusing behaviour of the blood cells in the spiral channel was consistent with that of the polystyrene microbeads. In other words, cells randomly distributed at the inlet migrated towards the inner wall along consecutive loops, and finally focused as a narrow band near the inner wall at the bifurcation.

As can be seen in Fig. 5B, although the focusing positions of the blood cells remain the same for all the blood samples with different dilutions, it is apparent that less diluted samples have a wider focusing band near the inner wall of the channel, which is due to intensive interactions between blood cells with higher concentrations. As was observed in the case of 5% haematocrit (HCT), these interactions caused a small portion of the blood cells to disturb the main particle focusing band and enter into the outer branch of the bifurcation. Evidently, the trapping capacity of the core of the Dean vortices near the inner wall is filled due to the high concentration of the blood cells which give rise the rest of the cells not to get affected by the inertial lift forces anymore, and exit from the outer outlet following the secondary flow.

Furthermore, the effects of the flow rate on the inertial focusing performance of the blood cells were studied (Fig. 5C). Basically, the width of the blood cells focusing band increases with the increment of the flow rate, which agrees with the trend of the polystyrene particles. It proves that the rigid polystyrene beads can appropriately mimic and predict the inertial focusing behaviour of the blood cells in the cell sorting microfluidic devices in which cell deformability is not a crucial design parameter.

View Article Online
DOI: 10.1039/C6LC00713A

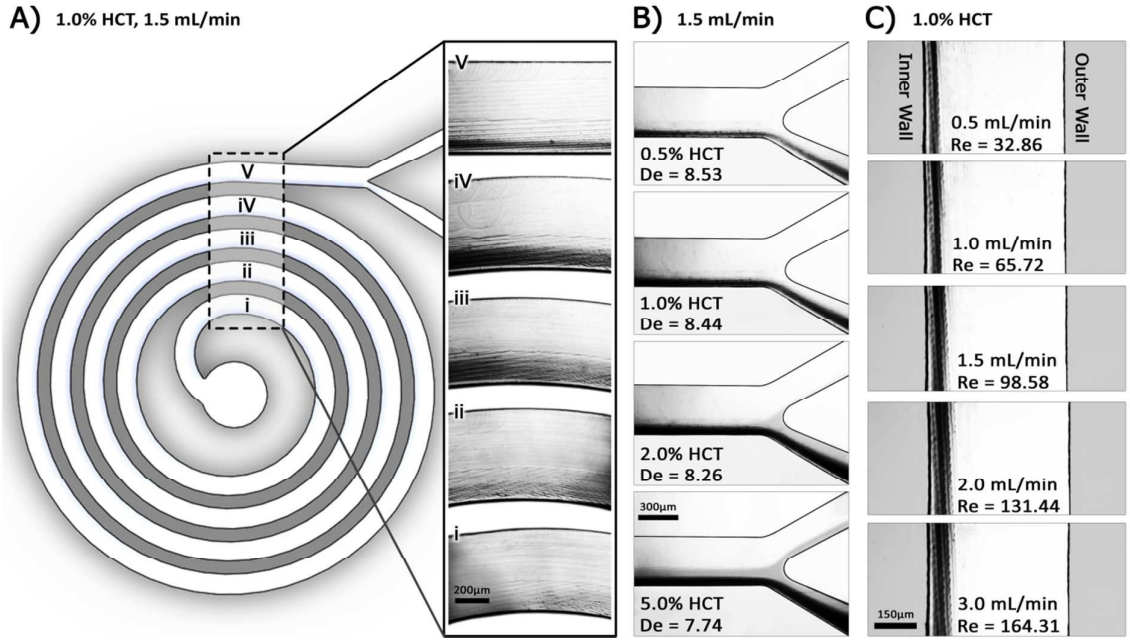

Fig. 5 Composite images illustrating the distributions of blood cells near the outlet of slanted spiral microchannel. (**A**) A compost image showing focusing of blood cells in different consecutive loops at flow rate of 1.5 ml/min. (**B**) The blood cells focusing at 1.5 mL/min with different dilutions of 9, 22.5, 45 and 90× corresponding to the HCT of 5%, 2%, 1% and 0.5%, respectively. (**C**) Blood cells distributions across the channel width at varying flow rates for HCT of 1%. Details of the calculations of *Re* and *De* in the slanted microchannel are provided in the supplementary info.

Moreover, as demonstrated in Fig. 6A-C, the blood streams entered the inner and outer branches of the bifurcation were collected in blood and plasma reservoirs respectively, Fig. 6E, and then put in a hemocytometer to count the concentration of the blood cells. The reject ratio is defined as $1 - c_p/c_i$, where c_p is the number of the blood cells in the unit volume of the collected plasma, and c_i is the number of the blood cells in the unit volume of the input blood sample (Fig. 6D). It was found that almost certainly 100% of the blood cells have been filtrated during the process by the proposed slanted spiral channel when HCT was 0.5% and 1%. This is further supported by the supplementary video 1. As can be seen in the movie, every droplet of the blood plasma collected from the outer branch is very clear, and the collected blood from the inner branch is dark red denoting a high concentration of the blood cells which are mostly RBCs. Fig. 6D demonstrates a marked decrease in the reject ratio with the increment of the concentration of the HCT. In this scenario, the wide focusing band of the blood cells pushes the overloading cells away the inner wall, directing a portion of them to the outer plasma stream.

View Article Online
DOI: 10.1039/C6LC00713A

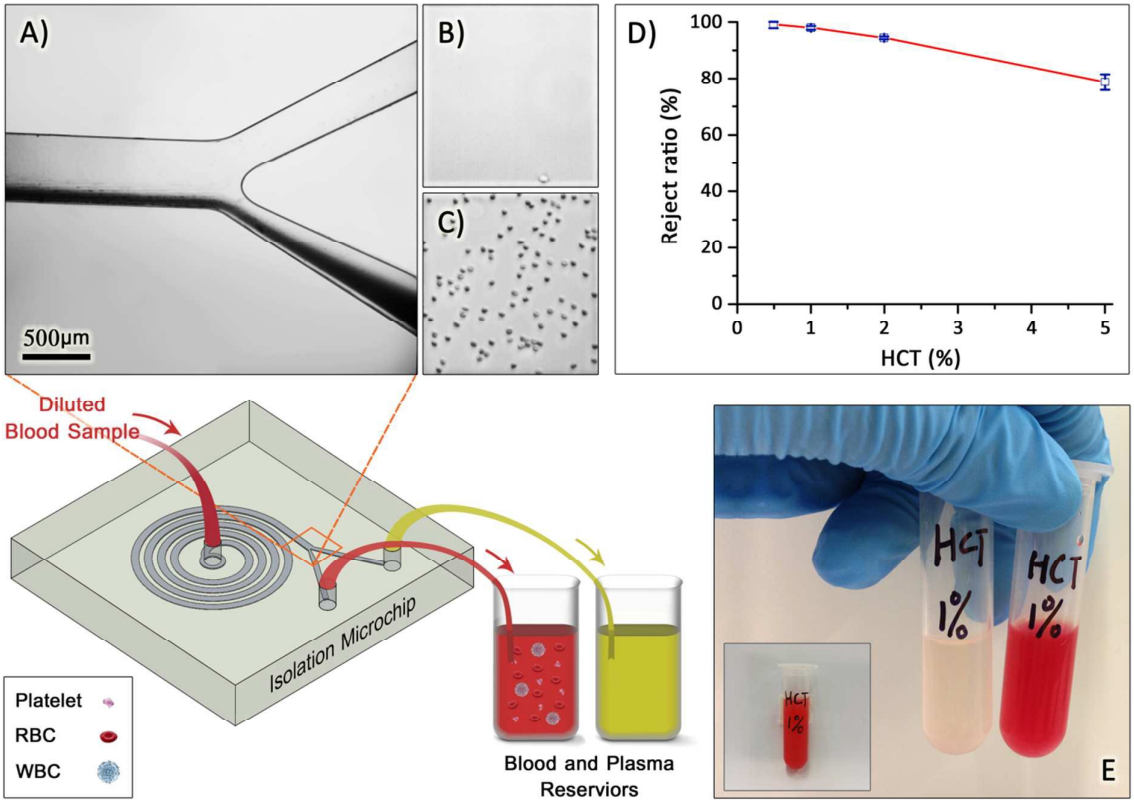

Fig. 6 Continuous blood plasma separations using the spiral channel with a trapezoidal cross-section. (**A-C**) Optical images of the blood cells focusing at the end of the spiral channel from which samples tested in hemocytometers. (**D**) The reject ratio (i.e., separation performance) of the spiral microdevice for blood samples with different HCTs. Error bars indicate the standard deviation of results from three tests. (**E**) Pictures of an initial diluted blood sample (inset) as well as samples collected from the inner outlet (plasma) and the outer outlet (blood cells), respectively.

4.3 Multiplexing design of the slanted spiral channels

A single spiral channel with trapezoidal cross-section can provide a high flow rate of 1.5 to 2 mL/min which is significantly higher than the previously reported microfluidic devices used for blood plasma extraction.[25, 30, 38] However, since the whole blood needs to be diluted before processing, and the volume of the blood sample is multiplied by the times of the dilution, a parallelization design to further scale up the total flow rate is desired. Table S4 compares the throughput of the current multiplex device with the microfluidic devices reported before. Currently, the parallelization designs are mostly based on microchannels with linear structure, e.g. straight [26] and serpentine [30] channels because a parallelization design for microchannels with complex nonlinear structure (e.g. spiral channel) is hard to implement, especially along the planar direction.

View Article Online
DOI: 10.1039/C6LC00713A

In this work, we built a multiplexing design for the slanted spiral channels and demonstrated its functionality for the blood plasma separation. Fig. 7A shows schematically the components of this design. 1) A 3D printed fluidic guide layer for delivery of diluted blood into individual spiral at uniform flow rates and collection of separated plasma from blood cells. 2) Two slabs of PDMS with embossed spiral channels (8 spirals in 1 layer), which are connected internally using a novel design (i.e., their outlets are all connected together) to boost the total throughput to 24 mL/min. 3) A base layer which is used to seal the bottom side of the spiral channels. It should be mentioned that more layers can be bonded together in the vertical direction to increase the throughput further through precise alignment and stacking.

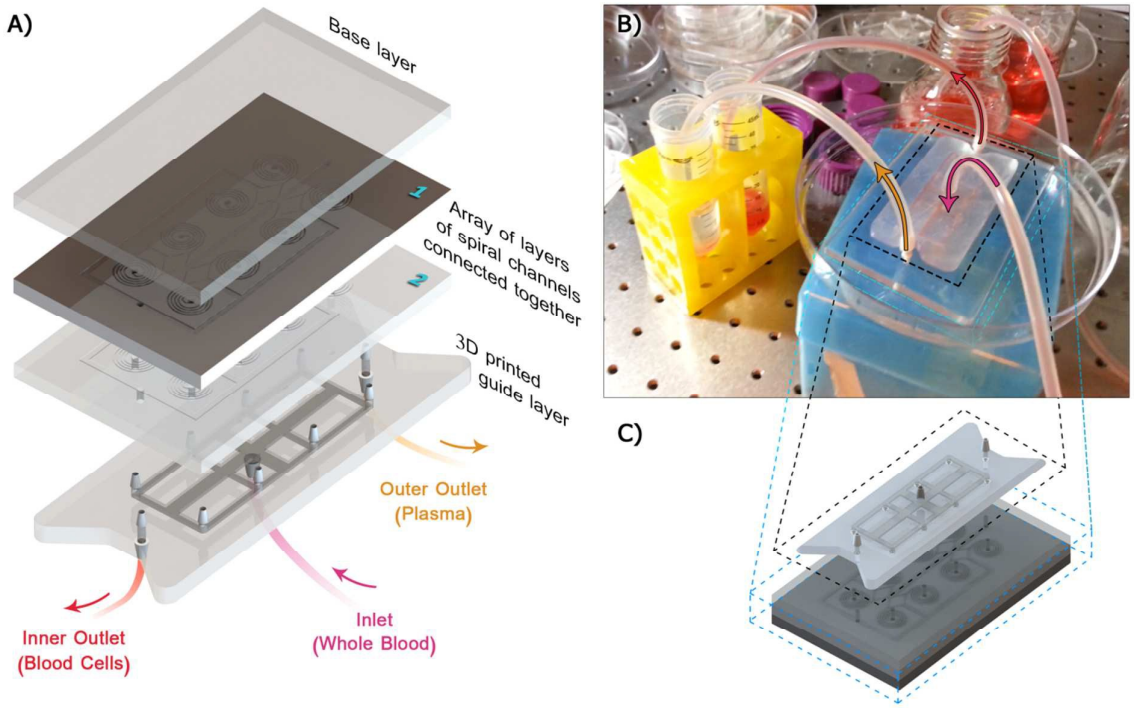

Fig. 7 Schematic illustration of a novel strategy for multiplexing spiral channels for ultra-fast blood plasma extraction. (**A**) The device consists of 16 spiral channels (8 spirals in each layer), one fluidic guide layer and one base layer. The PDMS layers with embossed spiral channels were fabricated using soft lithography approach. The outlets of all spirals are connected together using internal fluidic channels. These layers can then be precisely positioned and stacked (using plasma bonding) along the height direction to further multiply the total flow rate. A novel fluidic guide layer with conical pins was designed using 3D printing for blood infusion into the inlets of spiral channels. The base layer, either a flat PDMS or a glass sheet, was used to seal the spiral channels. (**B-C**) The Optical and schematic images of a multiplexed system during operation. The flow rate of this system can be as high as 24 mL/min. This throughput can be further scaled up through stacking more intermediate layers of spiral microchannels along the height direction.

View Article Online
DOI: 10.1039/C6LC00713A

Additionally, optimum design of the guide layer is very important for a leakage free process at high flow rates. In our design, the guide layer has three ports devised on its upper surface. The middle port is to infuse the blood sample into the spiral channels, and the two other ports are to collect the separated blood plasma and blood cells as shown in Fig. 7C. On the lower surface of the guide layer, there are eight conical ports which can be directly connected into the inlets of the spiral channels and seal them properly (Fig. 7A). In the current work, the multiplex microfluidic device with two layers of eight parallel spiral channels was fabricated, and its functionality on blood plasma separation was tested at an extremely high total flow rate of 24 mL/min. The working unit is shown in Fig. 7B. The multiplexed microfluidic device works very well for the blood plasma separation and can provide an excellent separation performance (see supplementary video 2).

5. Conclusions

In this work, we developed the multiplexing of the spiral microchannels with trapezoidal cross-section for ultra-fast plasma separation. First, particle inertial focusing performance in the designed slanted spiral channel was investigated using the differently-sized (3.0, 4.16 and 9.9 μm in diameter) polystyrene beads under different flow rates (0.5 to 3 mL/min). Flow rates ranging from 1.5 to 2 mL/min was found to be optimal for the microparticle filtration. Then, we investigated the effects that impact blood cells in the slanted spiral channel, including the focusing behaviour of blood cells in different loops of the spiral channels, the effects of blood cells concentration (HCT) and the flow rate on the blood cells inertial focusing. Blood plasma separation was conducted, and the separation performance of the spiral channels was measured. It was found that the reject ratio of the slanted spiral channel was almost surely 100% for the HCT of 0.5% and 1% under an optimal flow rate of 1.5 mL/min. However, the reject ratio decreases sharply by increasing the HCT. Finally, the parallelization design of the slanted spiral channels was conducted to further scale up the total flow rate. The designed and fabricated parallelized microfluidic devices consists of eight spiral channels in each of its intermediate layers, and can provide a total flow rate as high as 24 mL/min. The whole-blood equivalent flow rate under these conditions is ~ 530 μL/min, which means that the multiplex microdevice can process one millilitre of whole blood in less than one minute. We envisage that the proposed microfluidic device with multiplex spiral channels would be an excellent candidate for continuous high-throughput blood plasma

View Article Online
DOI: 10.1039/C6LC00713A

separation, and the design scheme will be instructive for parallelization design of non-linear microchannels with more complex structures.

Acknowledgements

We greatly appreciate A/Prof Ronald Sluyter, Illawarra Health and Medical Research Institute (IHMRI), University of Wollongong for the technical assistance of blood extraction to support this work. This work was performed (in part) at the NSW and South Australian node of the Australian National Fabrication Facility under the National Collaborative Research Infrastructure Strategy to provide nano- and micro-fabrication facilities for Australia's researchers.

References

1. H. W. Hou, A. A. S. Bhagat, W. C. Lee, S. Huang, J. Han and C. T. Lim, *Micromachines*, 2011, **2**, 319-343.
2. S. Tripathi, Y. B. V. Kumar, A. Prabhakar, S. S. Joshi and A. Agrawal, *Journal of Micromechanics and Microengineering*, 2015, **25**, 083001.
3. M. Kersaudy-Kerhoas and E. Sollier, *Lab Chip*, 2013, **13**, 3323-3346.
4. K. Aran, A. Fok, L. A. Sasso, N. Kamdar, Y. Guan, Q. Sun, A. Ündar and J. D. Zahn, *Lab on a Chip*, 2011, **11**, 2858-2868.
5. Z. T. F. Yu, K. M. Aw Yong and J. Fu, *Small*, 2014, **10**, 1687-1703.
6. J. Zhang, S. Yan, R. Sluyter, W. Li, G. Alici and N.-T. Nguyen, *Scientific reports*, 2014, **4**, Art No. 4527.
7. P. Gravesen, J. Branebjerg and O. S. Jensen, *Journal of Micromechanics and Microengineering*, 1993, **3**, 168.
8. G. M. Whitesides, *Nature*, 2006, **442**, 368-373.
9. P. K. Chaudhuri, M. E. Warkiani, T. Jing and C. T. Lim, *Analyst*, 2016, **141**, 504-524.
10. F. Petersson, L. Åberg, A.-M. Swärd-Nilsson and T. Laurell, *Analytical chemistry*, 2007, **79**, 5117-5123.
11. P. Augustsson, C. Magnusson, M. Nordin, H. Lilja and T. Laurell, *Anal Chem*, 2012, **84**, 7954-7962.
12. C. Iliescu, E. Barbarini, M. Avram, G. Xu and A. Avram, 2008.
13. C. Iliescu, G. Xu, E. Barbarini, M. Avram and A. Avram, *Microsystem Technologies*, 2008, **15**, 1157-1162.
14. A. A. S. Bhagat, H. Bow, H. W. Hou, S. J. Tan, J. Han and C. T. Lim, *Med. Biol. Eng. Comput.*, 2010, **48**, 999-1014.
15. J. Chen, J. Li and Y. Sun, *Lab Chip*, 2012, **12**, 1753-1767.
16. M. Kersaudy-Kerhoas and E. Sollier, *Lab on a Chip*, 2013, **13**, 3323-3346.
17. M. Sun, Z. S. Khan and S. A. Vanapalli, *Lab on a Chip*, 2012, **12**, 5225-5230.
18. X.-B. Zhang, Z.-Q. Wu, K. Wang, J. Zhu, J.-J. Xu, X.-H. Xia and H.-Y. Chen, *Analytical chemistry*, 2012, **84**, 3780-3786.
19. J. Moorthy and D. J. Beebe, *Lab on a Chip*, 2003, **3**, 62-66.
20. K. Loutherback, K. S. Chou, J. Newman, J. Puchalla, R. H. Austin and J. C. Sturm, *Microfluidics and nanofluidics*, 2010, **9**, 1143-1149.
21. D. W. Inglis, J. A. Davis, R. H. Austin and J. C. Sturm, *Lab on a Chip*, 2006, **6**, 655-658.

View Article Online
DOI: 10.1039/C6LC00713A

22. L. R. Huang, E. C. Cox, R. H. Austin and J. C. Sturm, *Science*, 2004, **304**, 987-990.
23. S. Choi, T. Ku, S. Song, C. Choi and J.-K. Park, *Lab on a Chip*, 2011, **11**, 413-418.
24. S. Choi, S. Song, C. Choi and J.-K. Park, *Lab on a Chip*, 2007, **7**, 1532-1538.
25. M. G. Lee, S. Choi, H. J. Kim, H. K. Lim, J. H. Kim, N. Huh and J. K. Park, *Applied Physics Letters*, 2011, **98**, 253702.
26. A. J. Mach and D. Di Carlo, *Biotechnology and bioengineering*, 2010, **107**, 302-311.
27. M. E. Warkiani, L. Wu, A. K. P. Tay and J. Han, *Annual Review of Biomedical Engineering*, 2015, **17**.
28. A. R. C. B. Service, Blood donation, http://www.donateblood.com.au/learn#how-donation-works, March 2016).
29. J. Zhang, S. Yan, D. Yuan, G. Alici, N.-T. Nguyen, M. E. Warkiani and W. Li, *Lab on a Chip*, 2016, **16**, 10-34.
30. J. Zhang, S. Yan, W. Li, G. Alici and N.-T. Nguyen, *RSC Advances*, 2014, **4**, 33149.
31. A. A. S. Bhagat, S. S. Kuntaegowdanahalli, N. Kaval, C. J. Seliskar and I. Papautsky, *Biomedical microdevices*, 2010, **12**, 187-195.
32. A. A. S. Bhagat, S. S. Kuntaegowdanahalli and I. Papautsky, *Lab Chip*, 2008, **8**, 1906-1914.
33. E. W. Kemna, R. M. Schoeman, F. Wolbers, I. Vermes, D. A. Weitz and A. van den Berg, *Lab on a Chip*, 2012, **12**, 2881-2887.
34. W. C. Lee, A. A. S. Bhagat, S. Huang, K. J. Van Vliet, J. Han and C. T. Lim, *Lab on a Chip*, 2011, **11**, 1359-1367.
35. N. Nivedita and I. Papautsky, *Biomicrofluidics*, 2013, **7**, 054101.
36. H. W. Hou, M. E. Warkiani, B. L. Khoo, Z. R. Li, R. A. Soo, D. S.-W. Tan, W.-T. Lim, J. Han, A. A. S. Bhagat and C. T. Lim, *Scientific reports*, 2013, **3**, Art No. 1259.
37. J. Sun, M. Li, C. Liu, Y. Zhang, D. Liu, W. Liu, G. Hu and X. Jiang, *Lab on a chip*, 2012, **12**, 3952-3960.
38. N. Xiang and Z. Ni, *Biomedical microdevices*, 2015, **17**, 1-11.
39. M. E. Warkiani, B. L. Khoo, D. S.-W. Tan, A. A. S. Bhagat, W.-T. Lim, Y. S. Yap, S. C. Lee, R. A. Soo, J. Han and C. T. Lim, *Analyst*, 2014, **139**, 3245-3255.
40. L. Wu, G. Guan, H. W. Hou, A. A. S. Bhagat and J. Han, *Anal. Chem.*, 2012, **84**, 9324-9331.
41. G. Guan, L. Wu, A. A. Bhagat, Z. Li, P. C. Chen, S. Chao, C. J. Ong and J. Han, *Scientific Reports*, 2013, **3**, 1475.
42. G. Segre, *Nature*, 1961, **189**, 209-210.
43. G. Segre and A. Silberberg, *Journal of Fluid Mechanics*, 1962, **14**, 136-157.
44. J.-P. Matas, J. F. Morris and É. Guazzelli, *Journal of Fluid Mechanics*, 2004, **515**, 171-195.
45. J. Zhang, S. Yan, D. Yuan, G. Alici, N. T. Nguyen, M. Ebrahimi Warkiani and W. Li, *Lab Chip*, 2015, **16**, 10-34.
46. J. Zhou and I. Papautsky, *Lab Chip*, 2013, **13**, 1121-1132.
47. G. Guan, L. Wu, A. A. Bhagat, Z. Li, P. C. Chen, S. Chao, C. J. Ong and J. Han, *Sci Rep*, 2013, **3**, 1475.
48. E. S. ASMOLOV, *Journal of Fluid Mechanics*, 1999, **381**, 63-87.
49. D. Di Carlo, *Lab on a Chip*, 2009, **9**, 3038-3046.
50. S. Berger, L. Talbot and L. Yao, *Annual review of fluid mechanics*, 1983, **15**, 461-512.
51. S. S. Kuntaegowdanahalli, A. A. Bhagat, G. Kumar and I. Papautsky, *Lab Chip*, 2009, **9**, 2973-2980.
52. D. Di Carlo, D. Irimia, R. G. Tompkins and M. Toner, *Proceedings of the National Academy of Sciences*, 2007, **104**, 18892–18897.
53. M. E. Warkiani, A. K. Tay, G. Guan and J. Han, *Sci Rep*, 2015, **5**, 11018.
54. H. Amini, W. Lee and D. Di Carlo, *Lab Chip*, 2014, **14**, 2739-2761.
55. D. Di Carlo, D. Irimia, R. G. Tompkins and M. Toner, *Proc Natl Acad Sci U S A*, 2007, **104**, 18892-18897.
56. A. A. Bhagat, S. S. Kuntaegowdanahalli and I. Papautsky, *Lab Chip*, 2008, **8**, 1906-1914.

View Article Online
DOI: 10.1039/C6LC00713A

57. N. Xiang, H. Yi, K. Chen, D. Sun, D. Jiang, Q. Dai and Z. Ni, *Biomicrofluidics*, 2013, **7**, 44116.
58. C. Liu, C. Xue, X. Chen, L. Shan, Y. Tian and G. Hu, *Anal Chem*, 2015, **87**, 6041-6048.
59. L. Sprenger, S. Dutz, T. Schneider, S. Odenbach and U. O. Hafeli, *Biomicrofluidics*, 2015, **9**, 044110.
60. N. Xiang, Z. Shi, W. Tang, D. Huang, X. Zhang and Z. Ni, *RSC Adv.*, 2015, **5**, 77264-77273.
61. D. Di Carlo, *Lab Chip*, 2009, **9**, 3038-3046.